

Non-Newtonian Flows in Two dimensional T-junctions

H. M. Matos¹, P. J. Oliveira¹

¹Departamento de Engenharia Electromecânica, Universidade da Beira Interior,
Rua Marques D'Ávila e Bolama, 6200-001 Covilhã, Portugal

Abstract

A computational fluid dynamics simulation study has been carried out for steady and unsteady laminar flows in a planar 2D T-junction, using inelastic and viscoelastic non-Newtonian fluids.

The present work aims to quantify the effects of flow rate ratio, inertia and elasticity upon the main flow characteristics in a dividing T-junction geometry, namely the size of the two recirculation zones created near the bifurcation and the stress fields. In hemodynamics such flow complexities are related to the genesis and development of vascular diseases, like the formation of atherosclerotic plaques and thrombi.

This study is also a first attempt to apply viscoelastic rheological models in bifurcation flows such as those which are relevant in hemodynamics.

Introduction

Bifurcation flows are important in many engineering and bio-engineering applications. In engineering applications, bifurcations are commonly used in liquid distribution systems. However when the working fluid is composed by a mixture of a number of fluids and other materials like it may be found in dyeing processes in the textile industry or in the production process of paper, phase distribution in the main and the branch ducts is inevitably different, affecting the flow control and processing facilities downstream. In some situations, like in the petroleum industries, this phenomenon is advantageous and is used to accomplish the first stage of oil and gas phase separation, with attending improvement in the efficiency of the transport system [1].

In bio-engineering, bifurcation flow has strong relevance in hemodynamics, since it is well-known that vascular diseases tend to occur near the branches of arterial bifurcations [2, 3].

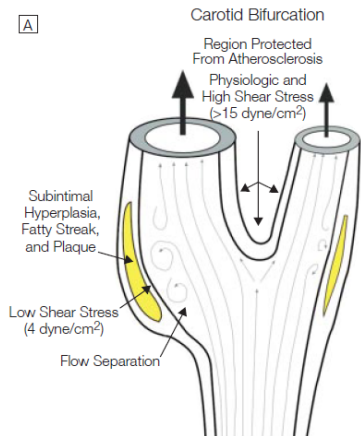


Figure 1 – Atherosclerotic plaques in a carotid bifurcation (Malek et al., 1999).

Atherosclerosis is the most common vascular disease. It occurs due to a damage of the endothelial cells in zones with small and oscillatory stress gradients [3], like those occurring in recirculation bubbles near arterial bifurcation (Fig. 1), and thus promoting the adhesion of platelets, red cells and lipoids into the endothelial wall (Fig. 2) [4].

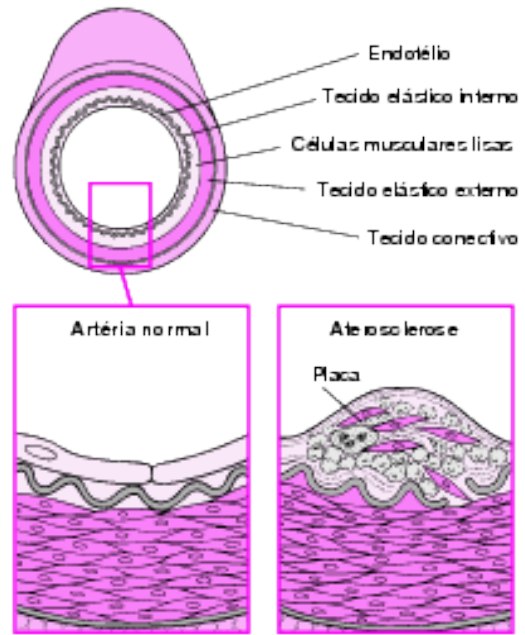


Figure 2 – Atherosclerotic plaque formation (<http://www.manualmerck.net/>).

One of the principal areas of research investigating the cause of atherosclerosis is the role of blood flow and its interaction with the artery wall through the action of fluid shear stress. In many studies the blood is modelled as a Newtonian fluid; however blood is a complex fluid that consists of a suspension of platelets, leucocytes and erythrocytes in plasma [5], and possesses therefore non-Newtonian properties. Blood exhibits a shear-thinning viscosity, is thixotropic and viscoelastic [6].

The present study aims to quantify the influence of inertia, elasticity, shear-thinning viscosity and flow rate ratio, on steady and unsteady laminar flows in a planar 2D T-junction. Inertia effects were varied through the Reynolds number ($Re = \rho \bar{u}_1 H / \eta$), from 50 to 1000. Elasticity properties were changed through the variation of Deborah number ($De = \lambda \bar{u}_1 / H$) and also the polymer concentration ($c = \eta_p / \eta_s$), whose increase corresponds to reducing the viscosity ratio ($\beta = \eta_s / \eta$). The shear-thinning viscosity follows the Carreau-Yasuda model in which the power law exponent was changed according to the intensity of viscosity variation. Finally the flow rate ratio ($\chi = Q_3 / Q_1$) varied from 0.1 to 0.9.

Numerical Simulation

Differential Equations

For an incompressible flow, the equations to be solved are the conservation of mass (Eq. (1)) and the conservation of linear momentum (Eq. (2)):

$$\nabla \cdot \mathbf{u} = 0 \quad (1)$$

$$\frac{\partial \rho \mathbf{u}}{\partial t} + \nabla \cdot (\rho \mathbf{u} \mathbf{u}) = -\nabla p + \nabla \cdot \boldsymbol{\tau} + \nabla \cdot (2\eta_s \mathbf{D}) \quad (2)$$

Where \mathbf{u} is the velocity, p is the pressure, ρ is the fluid density, \mathbf{D} is the rate-of-strain tensor and η_s is the solvent viscosity.

For the stress tensor in Eq. (2) we used different rheological constitutive models depending on whether the fluid is Newtonian, non-Newtonian inelastic or viscoelastic. For Newtonian fluids the stress tensor follows the Newton law for viscosity ($\boldsymbol{\tau} = 2\eta \mathbf{D} = \eta \dot{\boldsymbol{\gamma}}$), while for non-Newtonian inelastic fluids (Generalized Newtonian Fluids) the Carreau–Yasuda model [7] (Eq. 3) is followed to represent the viscosity variation with the shear rate.

$$\eta = \eta_\infty + (\eta_0 - \eta_\infty) \left[1 + (\Lambda \dot{\gamma})^a \right]^{-(n-1)/a} \quad (3)$$

In Eq. (3) η_0 and η_∞ are the zero and infinite shear rate viscosities, Λ is a constant time and n is the power law exponent. The magnitude of these parameters is obtained from [8].

For viscoelastic fluids the FENE-CR model (Eq. 4) proposed by Chilcot and Rallison [9] was used.

$$\boldsymbol{\tau} + \lambda \left(\frac{\nabla}{f(\boldsymbol{\tau})} \right) = 2\eta_p \mathbf{D} \quad (4)$$

λ is the relaxation time of the fluid at zero shear rate, the symbol ∇ denotes the Oldroyd upper convected derivative and the function $f(\boldsymbol{\tau})$ is given by:

$$f(\boldsymbol{\tau}) = (L^2 + (\lambda / \eta_p) \text{tr}(\boldsymbol{\tau})) / (L^2 - 3) \quad (5)$$

where L^2 is the extensibility parameter ($L^2 = 100$, constant) and tr represents the trace operator.

Numerical Method

We apply the finite-volume method on non-staggered meshes in which all variables are stored at the centre of cells forming the mesh [10]. The coupling between the velocity and stress fields employs the method of Oliveira et al. [11] later modified by Matos, et al. [12]. Spatial discretisation of the convective terms is accomplished with the high resolution scheme CUBISTA [13] and temporal discretisation of the unsteady term follows the three time level scheme [14]. The pressure-correction method employed is based on the SIMPLEC algorithm.

Geometry and Computational Mesh

The simulations were carried out in a 2D T-shaped geometry (Fig. 3) having a constant cross section area with height H . The flow conditions were similar to those of Miranda et al. [6]. At the inlet, a parabolic velocity

profile was imposed for steady flows, while a pulsating flow generated by a sinusoidal pressure gradient was imposed for unsteady flows:

$$-\frac{dp}{dx} = \rho K_s + \rho K_0 \cos(\omega t) \quad (6)$$

The ratio of oscillating and steady pressure gradients is $K_0/K_s = 2.585$ and the Womersley number is $\alpha = (H(\omega/\nu)^{1/2}) = 4.864$.

At the outlets, Neumann boundary conditions were imposed. The other boundary planes are solid walls where the no slip boundary condition was imposed. The mesh is the same of Matos et al. [12] where a study of mesh refinement can be found, it is formed by 12800 control volumes and the minimum space is 2.5×10^{-4} , while the time step is 5×10^{-3} .

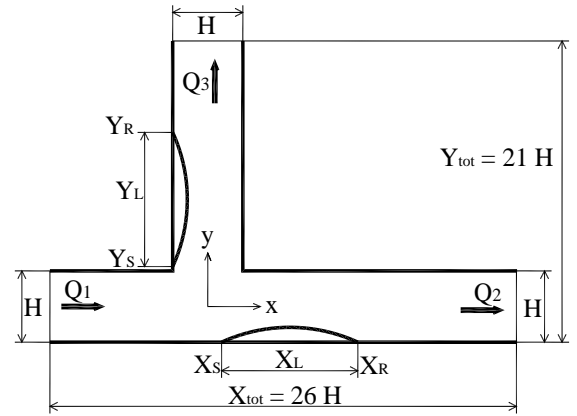


Figure 3 – Schematic representation of the simulation geometry.

Results and Discussion

The results presented are normalised: H length scale; $\eta U / H$ is the stress scale; and $2\pi / \omega$ is the time scale.

Depending of the flow parameters (Reynolds number, flow rate ratio, etc), T- Junction flows can promote the existence of one or two recirculation zones, which are represented in Fig. (3). The recirculation lengths change with inertia, elasticity, flow rate ratio, shear-thinning, for steady flows, while for unsteady flows they also change during the cycle.

In Fig. (4) the separation and reattachment points of both recirculations are presented for a viscoelastic flow with constant elasticity ($De = 1$, $\beta = 0.9$), inertia ($Re = 102$) and flow rate ratio ($\chi = 0.7$). This figure shows that the horizontal recirculation is not present during the whole cycle, while the vertical recirculation is always present. However, in the latter case an abrupt reduction in length occurs after the middle of the cycle, which is associated with the breakup of the recirculation into two vortices; the red line (square symbols) corresponds to the first reattachment point (unique before the division) and the purple line (circular symbols) to the second reattachment point associated with a second recirculation that tends to disappear later in the cycle.

Elasticity was defined with De and β for steady flows, and only with De (β constant) for unsteady flows. In the first case the reduction of β results in a increase of the polymer concentration ($c = (1 - \beta)/\beta$), and elasticity. Increasing De or reducing β for steady flows (Fig. 5), and increasing De for unsteady flows (Fig. 6), results on a decrease of the lengths of both recirculations, and an increase of the shear stress magnitude.

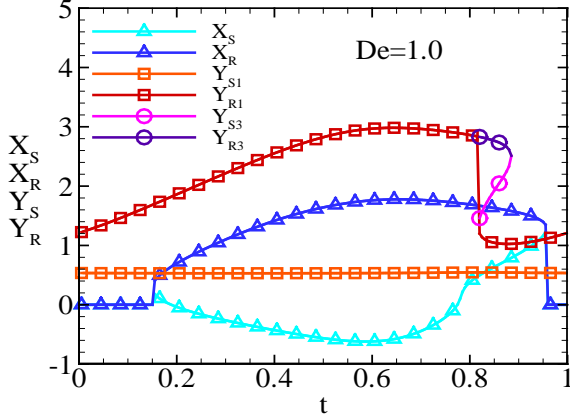


Figure 4 – X_S, X_R, Y_S, Y_R variation (unsteady viscoelastic flow).

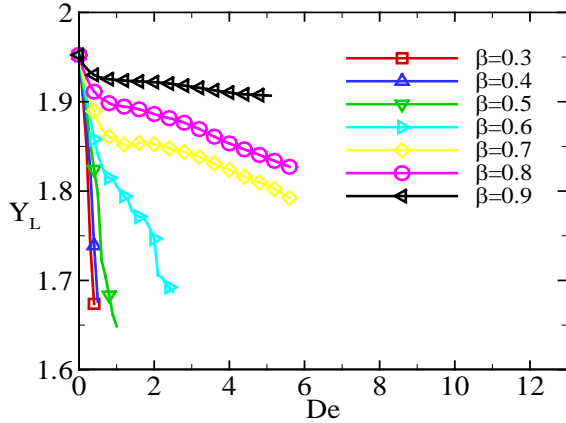


Figure 5 – Vertical recirculation length variation (steady viscoelastic flow).

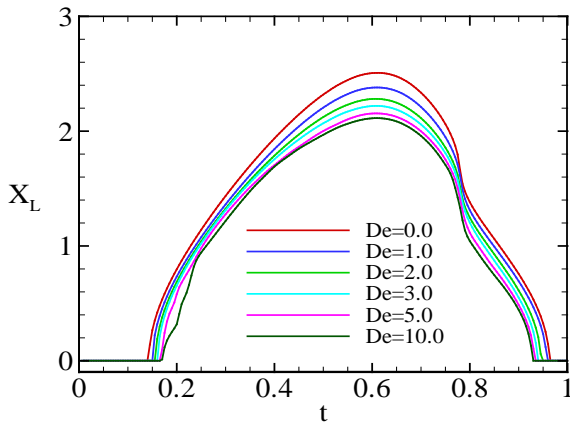


Figure 6 – Horizontal recirculation length variation (unsteady viscoelastic flow $\beta = 0.9$).

Inertial effects were analysed through the variation of Re for steady flows with both Newtonian and non-Newtonian inelastic fluids. The increase of Re results in higher recirculation lengths (Fig. 7) and shear stress magnitudes. In the case of non-Newtonian fluids there exists a viscosity dependency with the shear rate, which affects the calculation of the Reynolds number. In order to maintain a comparable Reynolds number between the Newtonian and non-Newtonian flow cases as in the results of Fig (7), the average velocity imposed at inlet should be such that the corresponding characteristic shear rate ($\dot{\gamma}_c = \bar{U}_1/0.5H$) yields a viscosity from Eq. (3) which results in the desired Re ($Re = \rho \bar{U}_1 H / \eta(\dot{\gamma}_c)$).

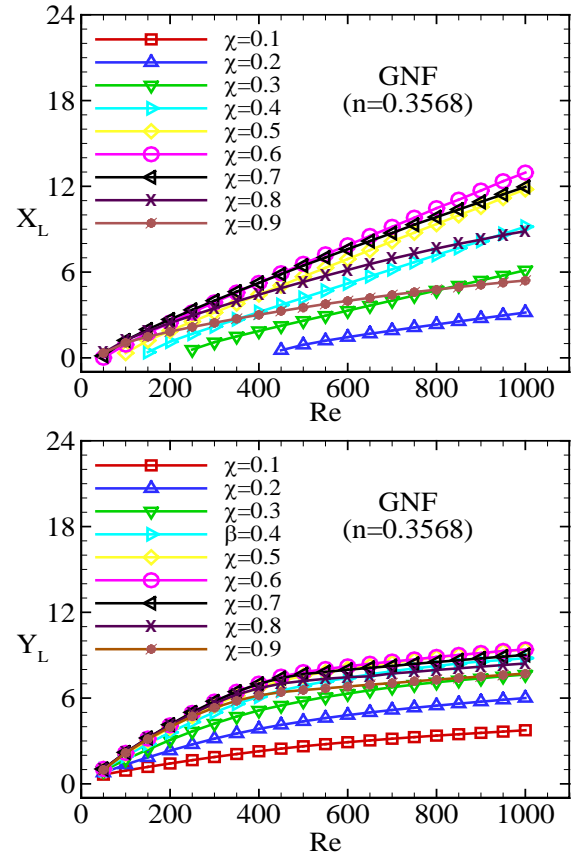


Figure 7 – Recirculation lengths variation with Reynolds and flow rate ratio (steady GNF flow).

From Fig. (7) is also possible to observe the influence of flow rate ratio. Initially, the increase of χ results in the increase of the recirculation lengths, however for $\chi > 0.6$, the opposite behaviour is observed. This conclusion also holds for the unsteady case, where the flow rate ratio variation was analysed for viscoelastic cases (Fig. 8). The results for both type of fluids also show an increase of the shear stress magnitudes with χ .

For flows with non-Newtonian inelastic fluids, the intensity of shear-thinning in viscosity was varied through the power law exponent (n) and analysed for both steady and unsteady flows. In these cases the increase of shear-thinning (decrease of n) results in a slight increase of

both recirculation lengths for the unsteady case (Fig. 9), while in the steady case a non monotonic behaviour was observed. The increase of shear-thinning also decreases the shear stress field.

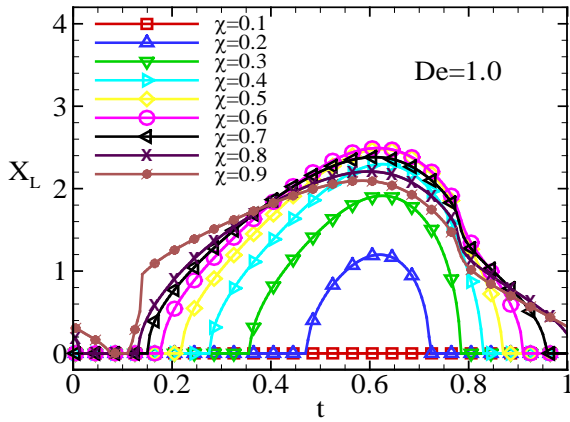


Figure 8 – Horizontal recirculation length variation with χ (unsteady viscoelastic flow).

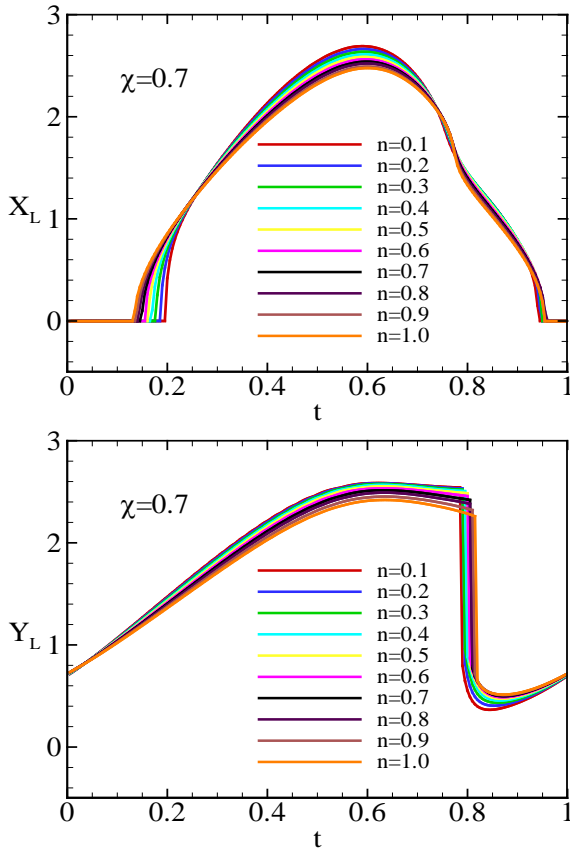


Figure 9 – Recirculation lengths variation with n (unsteady GNF flow).

The variation of the shear stress field with inertia, elasticity, shear-thinning viscosity and flow rate ratio was commented upon during the last section, however in all cases this field is characterized by low magnitudes of stresses in the recirculation zones and very high values in the re-entrante corners, as show in Fig. (10) for a steady viscoelastic flow ($De = 1$, $\beta = 0.9$, $Re = 102$, $\chi = 0.7$).

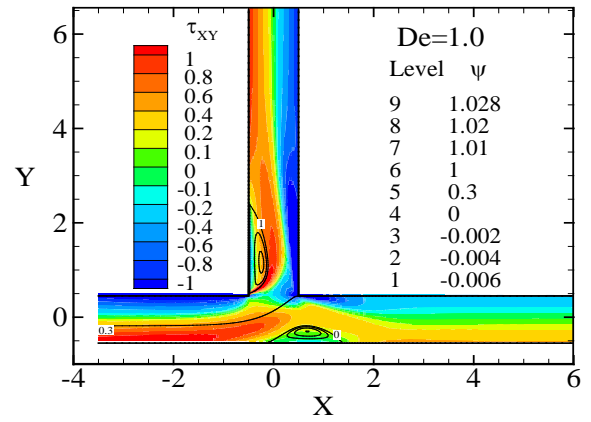


Figure 10 – Shear stress field (steady viscoelastic flow).

Conclusions

This study based on computer simulations generally shows a decrease of both recirculation lengths with elasticity and an increase with inertia for steady and unsteady flows, while the variation with flow rate ratio does not present a monotone behaviour. For non-Newtonian inelastic flows it is necessary to adopt a consistent Reynolds number in order to maintain the same value of Re as for the Newtonian case. When this is done, the influence of shear-thinning is minor.

References

1. Margaris, P.D., Chem. Eng. Proc., 46(2), 150, 2007.
2. Ku, D., Annu. Rev. Fluid Mech., 29, 399, 1997.
3. Berger, S.A. and Jou, L-D., Annu. Rev. Fluid Mech., 32, 347, 2000.
4. Liepsch, D., Moravec, S., Rastogi, A.K. and Vlachos, N.S., J. Biomech., 15(7), 473, 1982.
5. Anand, M. and Rajagopal, K. R., Int. J. Cardiovasc. Med. Sci., 4(2), 59, 2004.
6. Miranda A.I.P., Oliveira P.J. and Pinho F.T., Int. J. Numer. Meth. Fluids, 57(3), 295, 2008.
7. Carreau, P.J. Trans. Soc. Rheol., 16(1), 99, 1972.
8. Banerjee, R.K., Cho, Y.I. and Kensey, K.R., Int. J. CFD, 9(1), 23, 1997.
9. Chilcott, M.D. and Rallison, J.M., J. Non-Newt. Fluid Mech., 29, 381, 1988.
10. Oliveira, P.J., Ph.D. Thesis, University of London, 1992.
11. Oliveira, P.J. and Pinho, F.T., Numer. Heat Transfer B, 35(2), 295, 1999.
12. Matos, H.M.M., Alves, M.A. and Oliveira P.J., Numer. Heat Transfer B, 56(5), 351, 2009.
13. Alves, M.A., Oliveira, P.J. and Pinho, F.T., Int. J. Numer. Meth. Fluids, 41(1), 47, 2003.
14. Oliveira, P.J., J. Non-Newt. Fluid Mech., 101 (1-3), 113, 2001.

Acknowledgements

H.M. Matos wishes to acknowledge the financial support provided by FCT trough the grant SFRH/BD/18062/2004.